What a difference in biomechanics cardiac fiber makes

D. Gil[1], A. Borras[1], R. Aris[2], M. Vazquez[2], P. Lafortune[2], G. Houzeaux[2], J. Aguado[2], M. Ballester[3], C. H. Li[4], and F. Carreras[4]

1 Comp Vis Center-UAB; 2 Barcelona Supercomputing Center-CNS; 3 Med Dep, Lleida Univ; 4 Cardiac Imag Unit, Hosp Santa Creu i Sant Pau, IIB, Spain

Abstract. Computational simulations of the heart are a powerful tool for a comprehensive understanding of cardiac function and its intrinsic relationship with its muscular architecture. Cardiac biomechanical models require a vector field representing the orientation of cardiac fibers. A wrong orientation of the fibers can lead to a non-realistic simulation of the heart functionality.

In this paper we explore the impact of the fiber information on the simulated biomechanics of cardiac muscular anatomy. We have used the John Hopkins database to perform a biomechanical simulation using both a synthetic benchmark fiber distribution and the data obtained experimentally from DTI. Results illustrate how differences in fiber orientation affect heart deformation along cardiac cycle.

1 Introduction

[1]

Simulation of cardiac biomechanics requires the definition of a vector field representing the orientation of cardiac fibers inside a mesh of the geometry of the heart anatomy. Fiber information plays a key role, since an alteration of its distribution or orientation may lead to non-realistic incomplete models. There are two options for obtaining complete vector fields over the whole myocardial volume. Either using experimental measurements or relying on a rule-based mathematical model.

Experimental fiber orientation can be extracted from either histological studies or processing of DTI volumes. Histological cuts provide high resolution measurements of the local orientation of myocites [21, 7, 17]. Given that they provide sparse set of measurements, their use in cardiac mechanics simulations requires interpolation in order to obtain dense fields [7]. Such interpolation introduces artifacts in fiber orientation that are prone to hinder the simulation of biomechanics [4]. During the last decade, DT-MRI [16] has been established as the reference imaging modality for the rapid measurement of the whole cardiac architecture [5, 14, 3]. These models are dense and, thus, enable efficient solution of numerical problems. However, they provide a coarse representation that omits finer details

---

at some areas (such as papillary muscles) which might play a significant role in cardiac electrophysiology and mechanics. Whole-heart models with such fine details might be achieved by co-registering structural MR and DTMR data with histological data [11]. Still, a common limitation of fiber models obtained from experimental data is that they only provide *ex-vivo* measurements. Therefore they require volume registration for a general use in geometries different from the ones used for their computation.

Mathematical models of fiber orientation are defined in terms of the coordinates of myocardial material points in local systems. Among existing methods [18, 9, 12], the one described in [18] is the preferred for biomechanical simulations [1, 19, 4] because it allows defining fiber orientations in both ventricles. A main advantage of mathematical models of fibers is that they can be consistently computed *in-vivo* on any myocardial geometry. A main shortcoming is the validity of the mathematical assumptions for fully describing the complexity of cardiac fiber orientations everywhere. For instance, accurate definition of fibers at the septum or where both ventricles meet remains unknown [1].

In order to select the most appropriate model for simulations, it is mandatory to assess the impact that different fiber orientations have on final simulations. Recent studies have validated the mathematical model described in [18] for the simulation of the electrical propagation [1, 19]. The model has been successfully applied to the detection of arrythmia [19] and in [1] the authors report a qualitative comparison to DTI-based fibers. The comparison visually assesses discrepancies in, both, fiber orientation and simulated electrical propagations.

Even if it is presumed that discrepancies in fiber structure may significantly influence the simulation of the cardiac mechanics [1], as far as we know, there is a lack of quantitative studies. This paper explores the impact of the fiber information on the simulated biomechanics of cardiac muscular anatomy. We compare the canine DTI fiber model of the John Hopkins University, JHU, public data base [2] with the Streeter synthetic model [18]. The two fiber models are used in an electro-mechanical simulation of the heart [20]. Discrepancies between deformations are measured and related to differences in fiber orientations. Results show that the synthetic model presents a large discrepancy in the z-component of fibers that underestimates the longitudinal shortening of the left ventricle.

2 Computational Biomechanics

2.1 Cardiac Mesh Generation

Heart anatomy is given by the right and left ventricles and should exclude the atria. Atria and ventricles are separated by the basal loop, which complex geometry makes it difficult a fully automatic segmentation. Like existing approaches [13, 19, 4] we have developed a semi-automated solution using the open source software platform Seg3D [3]. A medical expert placed a set of key-points to locate

---

[2] http://gforge.icm.jhu.edu
[3] Seg3D: Volumetric Image Segmentation and Visualization, SCI

the heart valves on the MR image stack that conform the atrioventricular border. Key-point location was done on a set of image slices in coronal and sagittal views. Finally, a spline interpolation was used to segment the remaining slices of the volume. A list of voxels uniformly sampled over the volume mask was meshed as described in Section 2.3.

2.2 Fiber Distribution

We have chosen the following two approaches representative of mathematical and experimental fiber models:

Mathematical Fiber Model The local fiber orientation for each node has been calculated using the simulation package Chaste [10] as described in [12]. First, a map of the minimal distance from each node of the mesh to endocardium (d_{endo}) and epicardium (d_{epi}) is constructed, and the normalized thickness parameter e is defined:

$$e = \frac{d_{endo}}{d_{endo} + d_{epi}}$$

From that, the gradient of distance in each element is used to calculate the transmural direction. Finally, the so-called helix angle α is calculated to define the rotation of the fibre along transmural direction:

$$\alpha = R(1 - 2e)^n$$

where $R = \pi/3$ for the left ventricle and $R = \pi/4$ for the right ventricle. The parameters of this function are chosen to fit the observations reported in [18]. Following [1] we have considered a cubic ($n = 3$) and a linear ($n = 1$) model.

DTI-derived Fibers DT-MRI data is provided as a volume of three dimensional tensors. The primary eigenvector denotes the orientation of myocites on the given voxel. In this work we have used the public database of the JHU. This database provides MR data and such corresponding DTI information captured on a set of canine anatomies.

2.3 Efficient Biomechanical Model

The computational framework used is Alya System for Large Scale Computational Mechanics [6] which allows solving problems for nonhomogeneous anisotropic excitable media in thousands of processors running in parallel.

Electrophysiology and mechanical deformation are governed by sets of partial differential equations which are coupled via the free intracellular concentration and the stretch of the muscle fibers. The electrophysiology is modelled using the propagation equation of FitzHugh-Nagumo by a diffusion equation with nonlinear source terms [2] using the computational scheme described in [20]. The mechanical model implemented is based on a large strain total Lagrangian formulation. The total stress is the sum of a passive and an active contributions. The passive behavior is considered hyperelastic, orthotropic and compressible. A

local fiber-sheet-normal coordinate system is defined for every node of the mesh. The active part is transversely isotropic, with the active stress generated along the fiber direction [8].

A tetrahedra mesh of the list of voxels sampled on the segmented volume was generated using Tetgen [4]. Fiber field coming from DTI is defined at each node. In this way both problems, electrophysiology and mechanical deformation, are simulated on the same mesh, which in turn carries the original information of the DTI fibers. This procedure avoids interpolation errors that appears when each problem is solved in a different discrete mesh. Simulation models are implemented using explicit schemes with non-structured FEM meshes. In order to efficiently solve both problems the parallel coupled multi-physics solver of the Alya System was used. The parallelization of the code is based on automatic domain decomposition for distributed memory facilities.
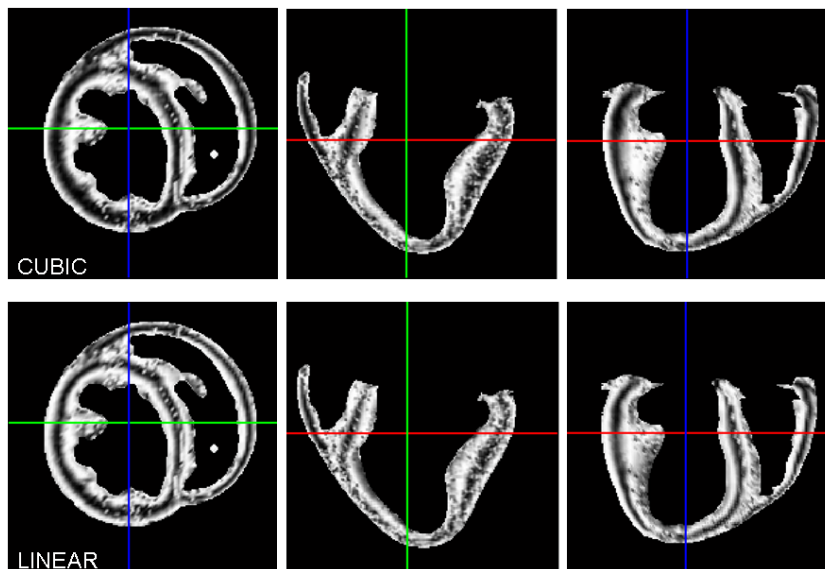

Fig. 1. Discrepancy between synthetic fibers and DTI.

3   Experiments

The goal of our experiments is to compare the cubic and linear fiber models with the fibers extracted from the DTI studies of the JHU public database in the context of cardiac mechanics simulations. In order to quantify the impact of discrepancies on simulated cardiac deformation, our experiments focus on

---

[4] http://tetgen.berlios.de/

two issues: discrepancies in fiber orientation and impact on simulated cardiac deformation.

3.1   Discrepancies in Fiber Orientation

Fibers computed using cubic and linear models have been compared to the fibers extracted from the DTI studies. For all models, fibers are given over the cardiac mesh segmented in Section 2.1. For each point in the mesh, synthetic fiber orientations are compared to DTI by means of the magnitude of the vector product, which, in the case of unitary vectors, corresponds to the sinus of the angle between them. Therefore it indicates the perpendicularity between fibers, 0 corresponding to parallel orientations and 1 to perpendicular ones. We will note this measure by $\mathcal{VP}_c$, $\mathcal{VP}_l$ for cubic and linear models, respectively.
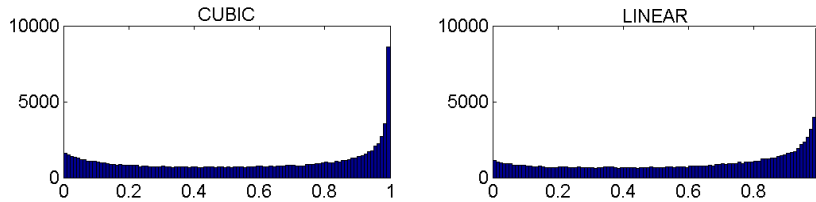

Fig. 2. Distribution of the discrepancy between synthetic fibers and DTI.

Figure 1, shows a Short Axis, SA, cut at basal level and a Long Axis, LA, cut of $\mathcal{VP}_c$ (top images) and $\mathcal{VP}_l$ (bottom images). We also show histograms of $\mathcal{VP}_c$ and $\mathcal{VP}_l$ for the whole myocardial volume in fig.2. We observe that, in both cases, there is a large discrepancy with DTI fibers. Synthetic orientations are in general perpendicular to DTI fibers (as shown in the histograms of fig.2). The difference in orientations is within 40.7 ± 27.6 degrees for the cubic model and within 44.6 ± 27.0 degrees for the linear one. Images in fig.1 indicate that discrepancies mainly occur at myocardial walls, septal unions, papillary muscles and trabeculae. Meanwhile, the similarity at mid-wall is high everywhere.

Figure 3 (a) visually compares the fiber directions for the 3 models for a sub-sampling of the myocardial mesh in SA (top) and LA (bottom) views. It is worth noticing that the main source of discrepancy is in the z-component of fibers, while x-y components follow similar orientations. The histograms in fig.3 (b) show the distribution of the z-component inside the myocardial volume. The cubic model is the one that differs most from DTI with a low z-component in general. Although the linear distribution is closer to DTI it fails to cover the most vertical vectors, mostly at trabeculae (see fig.1).

3.2   Impact on Simulated Cardiac Deformation

The 3 fiber models have been used to run the electro mechanical simulation described in Section 2.3. The deformation vector was computed every 4.2 ms for a
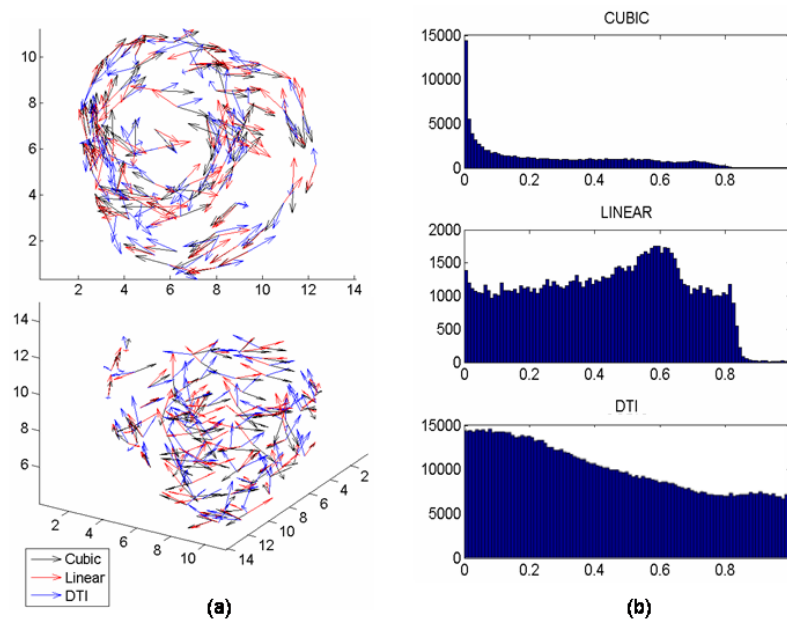
Fig. 3. Comparison of fibers for the three models.

period of 0.8 s. This time gap includes the whole systolic cycle and the beginning of the diastole. For each time t of the cardiac cycle, the simulation provided a vector field over each point of the segmented cardiac mesh that describes the deformation from time 0 to time t.
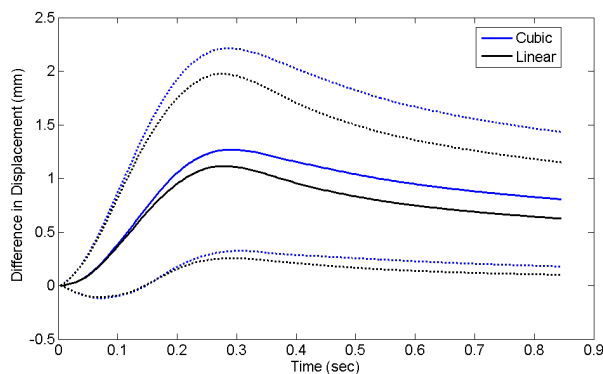

Fig. 4. Rank of displacements difference.

For each point in the mesh and time, we have computed the magnitude of the difference (in mm) between synthetic displacement vectors and DTI-based. Figure 4 shows the ranks (given by the mean ± standard deviation) of this differences as a function of time. The largest difference is achieved, for both models, around 0.3 seconds, which corresponds to the maximal myocardial contraction at end systole.

Figure 5 shows a snap shot of the deformed mesh at $t = 0.3$ seconds in LA view. The mesh at time 0 is also shown as a gray grid. Colors in the deformed mesh correspond to the potential of the electrical propagation. As reported in the literature [1], we do not observe significant differences in the electrical part, but a small delay the synthetic models. As suspected, fiber structure are decisive in the modelling of cardiac mechanics. The cubic model fails short in longitudinal contraction compared to the linear and DTI models. This is a direct consequence of its lack of z-component (see histogram in fig. 3). The longitudinal shortening of the linear model is closer to DTI shortening at basal level, although it underestimates the overall shortening. The basal septal level and papillary muscles undergo a significant motion in the DTI model that it is absent in the linear one. We attribute this discrepancy to a lack of the most vertical fibers in the linear model (see histogram in fig. 3).
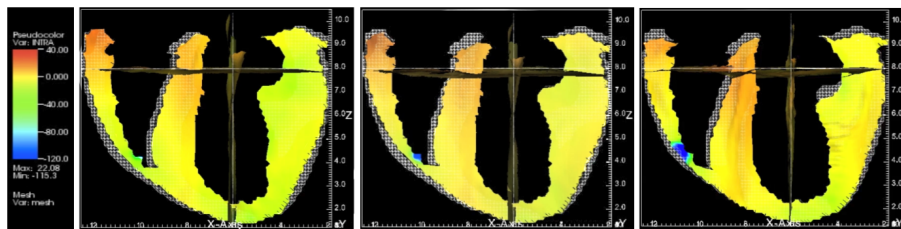

Fig. 5. Snap shot in LA view of the simulated deformations.

4   Conclusions

Accurate fiber orientation is crucial for getting realistic simulations of heart mechanics. Cubic and linear models underestimate the z component of fibers and, thus, motion at basal level (cubic) and papillary muscles (linear). It follows that such synthetic models produce simulations that do not correctly match the true motion. Our future research includes exploring the impact of discrepancies in clinical scores of the cardiac function (such as torsion) and analyzing recent mathematical models [15] based on the helical structure of the heart.

Acknowledgements

References

1. M. Bishop, P. Hales, and G.et al. Plank. Comparison of rule-based and dtmri-derived fibre architecture in a whole rat ventricular computational model. In *FIMH, LNCS*, volume 5528, pages 87–96, 2009.

2. Richard Fitzhugh. Impulses and physiological states in theoretical models of nerve membrane. *Biophysical Journal*, 1(6):445–466, July 1961.

3. C Frindel, J Schaerer, P Gueth, P Clarysse, Yue-Min Zhu, and M Robini. A global approach to cardiac tractography. In *ISBI*, pages 883 – 886, 2008.

4. V. Gurev, T. Lee, J. Constantino, and et al. Models of cardiac electromechanics based on individual hearts imaging data. *Biomech Mod Mechanobiology*, 10(3):295–306, 2011.

5. P. Helm, M. Faisal, M. I Miller, and R. L Winslow. Measuring and mapping cardiac fiber and laminar architecture using diffusion tensor mr imaging. *Ann N Y Acad Sci*, 1047:296–307, 2005.

6. G Houzeaux, R Aubry, and M VÃzquez. Extension of fractional step techniques for incompressible flows: The preconditioned orthomin(1) for the pressure schur complement. *Computers and Fluids*, 44(1):297–313, 2011.

7. P. Nielsen, I. Le Grice, B. Smail, and P. Hunter. Mathematical model of geometry and fibrous structure of the heart. *Am J Physiol.*, 260 (29):H1365–H1378, 1991.

8. M. Vazquez P. Lafortune, R.Aris and G. Houzeaux. Coupled parallel electromechanical model of the heart. *Int. J. Num. Meth. Biomed. Eng.*, 28(1):72–86, 2012.

9. C. S. Peskin. Fiber architecture of the left ventricular wall: An asymptotic analysis. *Comm on Pure and App Math*, 42 (1):79–113, 1989.

10. J. M. Pitt-Francis, P. Pathmanathan, and M. O.and et al. Bernabeu. Chaste: a test-driven approach to software development for biological modelling. *Comp Phys Comm*, 180(12):2452–2471, 2009.

11. G. Plank, R. Burton, P. Hales, and et al. Generation of histo-anatomically representative models of the individual heart: tools and application. *Phil Trans Royal Soc*, 367(1896):2257–2292, 2009.

12. M. Potse, B. Dube, J. Richer, and et al. A comparison of monodomain and bidomain reaction-diffusion models for action potential propagation in the human heart. *Trans. Biomed Eng*, 53 (12):2425–2435, 2006.

13. T.A. Quinn R. Casero, R.A.B. Burton and et al. Cardiac valve annulus manual segmentation using computer assisted visual feedback in three-dimensional image data. In *EMBC*, page WeBPo10.7, 2010.

14. D Rohmer, A Sitek, and G Gullberg. Reconstruction and visualization of fiber and laminar structure in the normal human heart from ex vivo diffusion tensor magnetic resonance imaging dtmri data. *Invest Radiol*, 42 (11):777–789, 2007.

15. P. Savadjiev, G. J. Strijkers, A. J Bakermans, and et al. Heart wall myofibers are arranged in minimal surfaces to optimize organ function. *Proc Natl Acad Sci*, 109(24):9248–9253, 2012.

16. D F Scollan, A Holmes, R Winslow, and J Forder. Histological validation of myocardial microstructure obtained from diffusion tensor magnetic resonance imaging. *Am J Physiol*, 275(6 Pt 2):H2308–18, Dec 1998.

17. C Stevens, E Remme, I LeGrice, and P Hunter. Ventricular mechanics in diastole: material parameter sensitivity. *J Biomech*, 36:737–748, 2003.

18. D D Streeter, H M Spotnitz, D P Patel, and et al. Fiber orientation in the canine left ventricle during diastole and systole. *Circ Res*, 24 (2):339–347, 1969.

19. F. Vadakkumpadan, H. Arevalo, A. J. Prassl, and et al. Image-based models of cardiac structure in health and disease. *Wiley Interdiscip Rev Syst Biol Med*, 2(4):489–506, 2010.
20. M. Vazquez, R. Aris, G. Hozeaux, and et al. A massively parallel computational electrophysiology model of the heart. *Int. J. Num. Meth. Biomed. Eng.*, 27:1911–1929, 2011.
21. F.J. Vetter and A.D McCulloch. Three-dimensional analysis of regional cardiac function: a model of rabbit ventricular anatomy. *Prog. Biophys. Mol. Biol*, 69:157 − 183, 1998.